Computational investigation of the aerodynamic performance of reversible airfoils for a bidirectional tidal turbine

To cite this article: K E T Giljarhus *et al* 2021 *IOP Conf. Ser.: Mater. Sci. Eng.* **1201** 012003

Computational investigation of the aerodynamic performance of reversible airfoils for a bidirectional tidal turbine

K E T Giljarhus[1], G S Shariatpanahi[1] and O A Frøynes[2]

[1] University of Stavanger, Stavanger, Norway
[2] Framo Innovation AS, Bergen, Norway

E-mail: knut.e.giljarhus@uis.no

Abstract. A reversible airfoil is an airfoil that has equal performance when the flow is reversed. Such airfoils are relevant for many different applications, including use in ventilation fans, helicopter rotors, wind turbines and tidal turbines. Compared to traditional airfoils, reversible airfoils have different performance characteristics and have been less explored in the scientific literature. This work investigates the aerodynamic performance of some selected reversible airfoils using computational fluid dynamics. The selected airfoils are based on existing NACA 6 profiles and a profile using B-spline parameterization. The results show reduced performance for the reversible airfoils compared to a unidirectional airfoil. Of the investigated airfoils, the B-spline airfoil has the highest performance, with a maximum aerodynamic efficiency which is 87 % of the unidirectional design.

1. Introduction

A tidal turbine design needs to consider the harsh environment of the sea. Reducing the number of moving parts is therefore desirable. Compared to wind flow, a tidal stream is relatively predictable with small directional variance. This makes it attractive to avoid a yaw gear on the turbine and instead use a reversible airfoil, allowing the turbine to operate with equal performance in both ebb and tide. In addition to tidal turbines, reversible airfoils are also relevant in other areas, such as axial ventilation fans[1], helicopter rotors[2] or building-augmented wind turbines[3].

Li et al.[4] used 3D CFD simulations to investigate the influence of blade curvature on a bidirectional tidal turbine. They found that by increasing the curvature of the blade the low-pressure surface area of the blade could be increased resulting in increased lift. Only a small number of curvatures were considered and little information on the actual blade design and computational setup were given. Nedyalkov and Wosnik[5] designed a new class of bidirectional airfoils using stretched circles at the leading and trailing edges, connected by a straight line. This gives a reversible airfoil shape parameterized by three parameters. The performance of the various configurations was studied by performing 2D CFD simulations. They demonstrated modest performance gains compared to a reversible NACA airfoil, with a maximum aerodynamic efficiency of 25 %. The performance in off-design conditions was not considered. In [6], experiments and fully-resolved 3D simulations were performed for a three-bladed tidal turbine design with both unidirectional and reversible airfoils. a bidirectional design. They also used

NACA airfoils in their reference unidirectional design. They found a decrease in lift and increase in drag between 14-25 % for the considered reversible airfoils. However, the full simulations only gave a reduced power production of 1.6 % at the optimal tip speed ratio. It should be noted that they used symmetric NACA airfoils without any camber for the unidirectional, which is not optimal in terms of maximum aerodynamic performance.

The purpose of the current work is to evaluate various reversible airfoil designs in terms of the aerodynamic performance in both optimal and off-design conditions. Additionally, the aim is to devise and validate a computational method and performance parameters suitable for use in an optimization procedure.

2. Airfoil geometry

This section presents the different airfoils considered in this study. To analyze the effectiveness of an airfoil, the forces acting upon it are divided into two components; the drag, which acts in the direction parallel to the incoming flow and the lift, which acts in the direction perpendicular to the incoming flow. These forces are typically made non-dimensional in the form of drag and lift coefficients, which are defined as

$$C_D = \frac{F_D}{\frac{1}{2}\rho U_\infty^2 CW} \tag{1}$$

$$C_L = \frac{F_L}{\frac{1}{2}\rho U_\infty^2 CW}. \tag{2}$$

Here, F_D and F_L are the forces in the drag and lift directions, respectively, ρ is the fluid density, U_∞ is the freestream velocity, C is the airfoil chord length and W the width of the airfoil section.

With respect to optimal performance of an airfoil for a turbine blade, there are many factors to be considered. The main driving factor is the aerodynamic efficiency, $\epsilon = C_L/C_D$. The angle of attack where the effectiveness reaches its maximum is typically chosen as the design point for the airfoil section in a turbine blade. This point is reached at an angle of attack lower than the angle of attack with the maximum lift coefficient (the stall point). An example of this is shown in Figure 1. To reduce extreme loads on the blade, the performance in off-design conditions should also be considered. If the design point is too close to the stall point, the turbine could operate in stall more often than necessary which would reduce the life time. Additionally, if the slope of the performance curve from the design point to the stall point is large, it could lead to high stresses in the turbine and significant drop-offs in performance[7]. These factors can be expressed mathematically as

$$\Delta\alpha = \alpha_{\text{stall}} - \alpha_{\text{design}} \tag{3}$$

$$S_\epsilon = \frac{\epsilon_{\text{design}} - \epsilon_{\text{stall}}}{\Delta\alpha} \tag{4}$$

These two parameters are also illustrated in Figure 1. A turbine design robust to off-design conditions is obtained with airfoils having a high $\Delta\alpha$ and a low S_ϵ.

2.1. Baseline airfoil, NACA65-415

The baseline airfoil used for comparison is the uni-directional NACA 65-415 airfoil. NACA airfoils represent airfoil shapes using a series of digits representing the geometric properties of the airfoil. For the present airfoil, 6 designates the series, 5 is the location of the minimum pressure in tenths of chord length, 4 gives the design lift coefficient as 0.4 and the last two digits give the thickness in percentage of chord length. The airfoil shape can be seen in Figure 2.

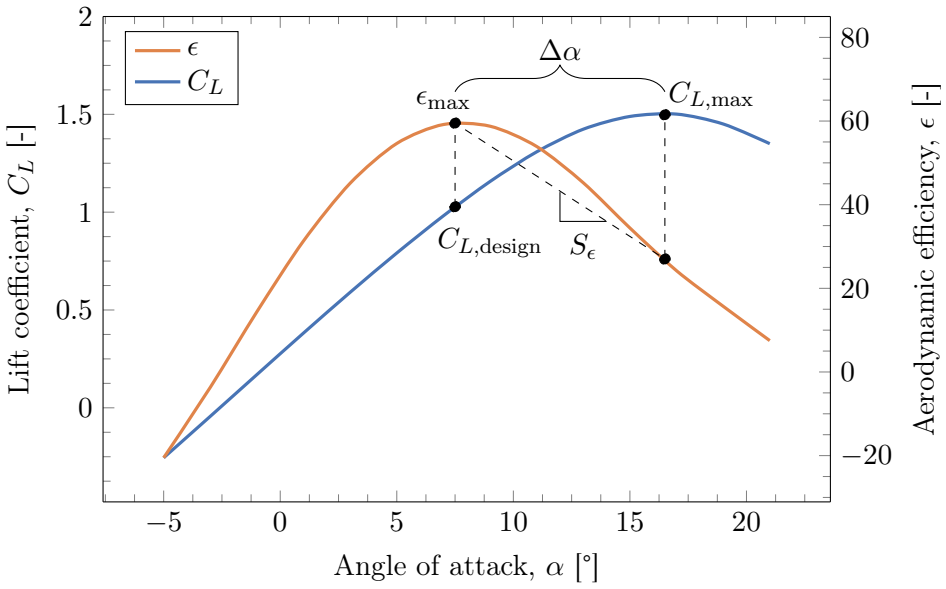

Figure 1: Performance curves and off-design performance parameters for an airfoil.

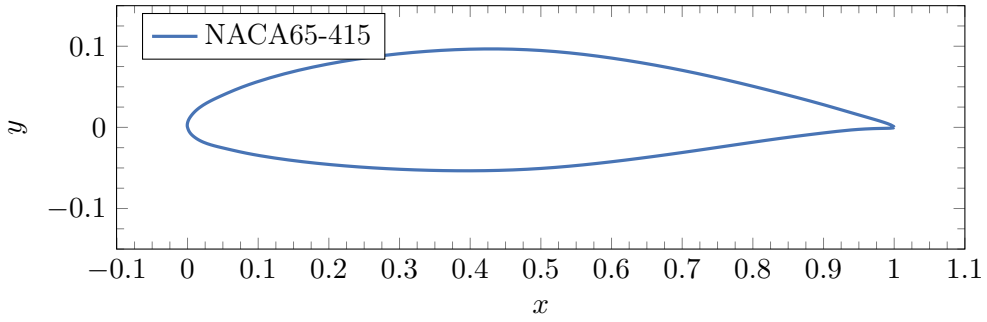

Figure 2: Geometry of the baseline airfoil, NACA 65-415.

2.2. NACA bisymmetric airfoil, SYM65-015
This geometry is a bisymmetric version of the baseline airfoil. The NACA 65-015 is used as the starting point, as it is symmetric around the x-axis. Next, the first 40 % of the airfoil is mirrored around the y-axis at the half chord length. The two parts are finally connected by a straight line. The resulting profile is shown in Figure 3. Also shown is an elliptic airfoil shape, and it is evident that the two profiles are very similar.

2.3. NACA reversible airfoil, ASYM65-415
This geometry is an asymmetric version of the baseline airfoil. It is built by taking the NACA 65-415 profile for the upper profile, then flipping that profile both vertically and horizontally to generate the lower part. The resulting profile is shown in Figure 4.

2.4. B-spline parameterized airfoil
Finally, a parameterized reversible airfoil shape is considered. This is done to later connect the computational method to an optimization routine. There are many different way to parameterize an airfoil. In [8], a review of these techniques are given. Regardless of which technique is considered, they should minimize the number of parameters and be able to cover a wide range of

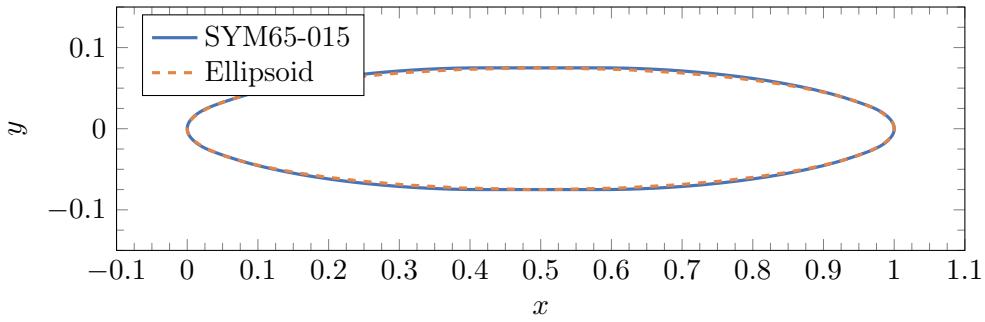

Figure 3: Geometry of the SYM65-015 airfoil, compared against an elliptic shape.

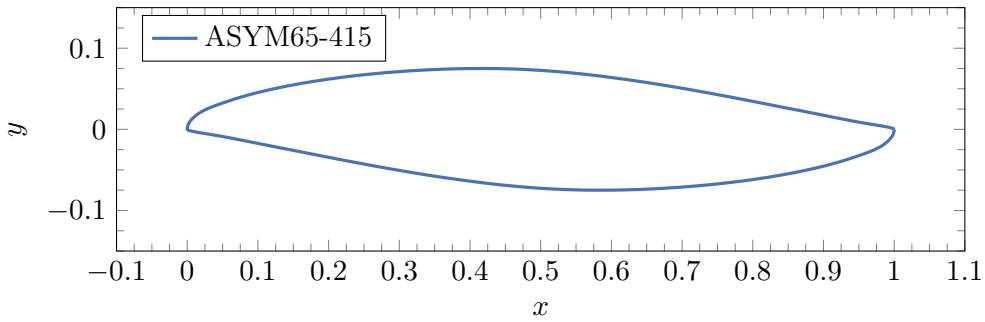

Figure 4: Geometry of the reversible, asymmetric version of the NACA 65-415, where the upper profile is rotated to generate the lower profile.

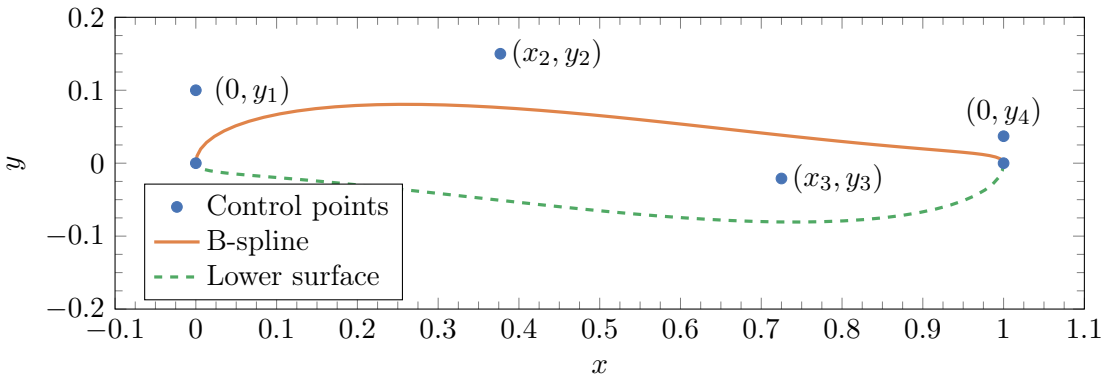

Figure 5: Illustration of control points and B-spline used for airfoil shape parameterization.

existing airfoils. In this work, the technique used in [1] is adopted. The airfoil is parameterized by a sixth degree B-spline using six control points, as shown in Figure 5. The end points are fixed to (0,0) and (1,0), and the second and second to last points are only allowed to move along the y-axis. This gives a total of six parameters for a single airfoil realization. The airfoil considered here has control point coordinates $y1 = 0.100$, $x2 = 0.377$, $y2 = 0.150$, $x3 = 0.725$, $y3 = -0.021$, $y4 = 0.037$. This design is based on engineering judgement to provide a starting point for later optimization. To increase the lift a blunter nose is chosen, but not too blunt as this will increase the drag and give stall at an earlier angle of attack. The drag could also be reduced by creating a thinner airfoil, but this is not desirable from structural considerations.

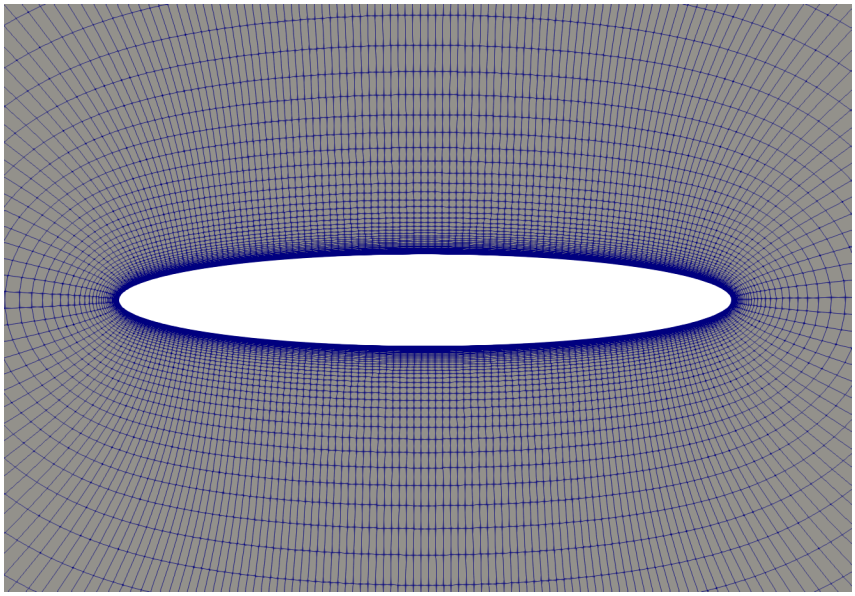

Figure 6: Computational grid with O-grid structure for the SYM65-015 airfoil.

3. Computational fluid dynamics

The simulations in this work are performed in the open-source CFD simulation software OpenFOAM, version 7[9, 10].

Simulations are performed with a Reynolds-averaged Navier-Stokes (RANS) turbulence model, more specifically the Spalart-Allmaras turbulence model [11]. The SIMPLE algorithm is used for pressure-velocity coupling. For discretization, second-order discretization schemes are used. For the convective terms, a second-order central-upwind scheme with a Sweby limiter is used [12]. The residual limit for the solution process is set to 1×10^{-6} for all variables.

3.1. Computational mesh and boundary conditions

Construct2D is an elliptic grid generator to create 2D grids for airfoil simulation[13]. Construct2D is chosen since it has a simple text-based input format allowing for easy automation of high-quality grids. The grids are generated in Plot3D format, which can then be converted to the OpenFOAM grid format using the built-in `plot3dToFoam` utility in OpenFOAM.

The overall computational domain as well as the mesh close to the airfoil is shown in Figure 6. The mesh is an O-grid with radius 100 times the chord length of the airfoil. Freestream boundary conditions are used on the outer edge of the computational domain, and no-slip conditions on the airfoil surface. The Reynolds number, $\mathrm{Re} = UC/\nu$, is set to 1×10^6, unless otherwise noted.

3.2. Mesh sensitivity

A mesh study is performed to find a suitable grid for the remainder of the work. Since the aim is to eventually use the CFD simulation in an optimization process, a good compromise between simulation speed and accuracy is required. The sensitivity study is performed for the SYM65-015 airfoil at an angle of attack of 6°.

Table 1 shows the mesh parameters and the resulting drag/lift coefficients. The grids are made by successively increasing all the mesh parameters; the number of points on the airfoil surface, the mesh spacing near the edges and the number of points in the fluid volume. The grid cell closest to the surface is kept constant to maintain a non-dimensional distance, y^+, to the surface lower than 1.

There are minor differences between very coarse, coarse and medium grids, and no difference between the medium and fine grids (to the specified number of decimals), indicating that the medium mesh size is sufficient. A single simulation with this grid only takes around 30 seconds, running on an Intel Xeon Gold 6148 processor with 20 2.4 GHz cores.

Table 1: Sensitivity of mesh size.

Grid	Surface points (-)	Edge spacing (mm)	Volume points (-)	Drag (-)	Lift (-)
Very coarse	125	4×10^{-3}	50	0.01491	0.4368
Coarse	188	3×10^{-3}	75	0.01423	0.4429
Medium	250	2×10^{-3}	100	0.01491	0.4368
Fine	375	1.5×10^{-3}	150	0.01491	0.4368

3.3. Validation

To validate the computational setup, the simulations for the SYM65-015 airfoil at a Reynolds number of 2×10^6 were compared against experimental results from [14] for an elliptic airfoil. The comparison to an elliptic airfoil is justified based on the similarity shown in Figure 3. Additionally, since experimental results for the drag coefficient are not available, simulations were also performed for a NACA 0012 airfoil for a Reynolds number of 6×10^6. For this airfoil, extensive experimental data and CFD simulation data are available[15, 16].

The lift and drag coefficients over a range of angle of attacks are shown in Figure 7. The simulated results are in very good agreement with the experiments. As expected, the lift for the bisymmetric airfoil is lower than the NACA 0012 airfoil, and the drag is higher due to the thicker airfoil and the less efficient blunt trailing edge. This is further illustrated by Figure 8, which shows the separation flow pattern at the trailing edge for the bisymmetric airfoil.

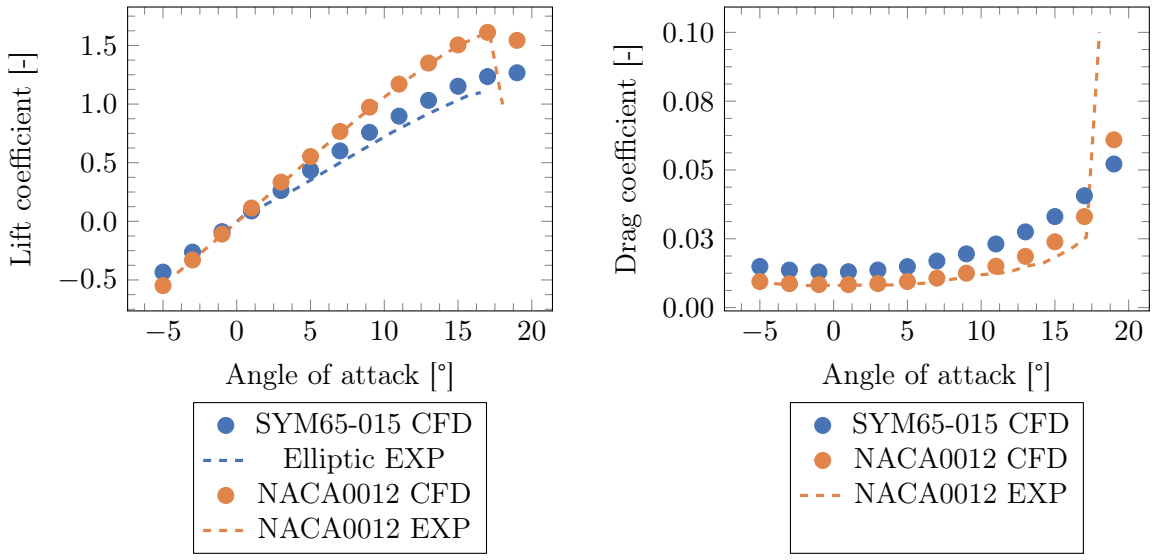

(a) Lift coefficient. **(b)** Drag coefficient.

Figure 7: Simulated lift coefficients for elliptic airfoil, compared against experimental results[14]. Also included are simulated lift and drag coefficients for the NACA 0012 airfoil, compared against experimental results[15, 16].

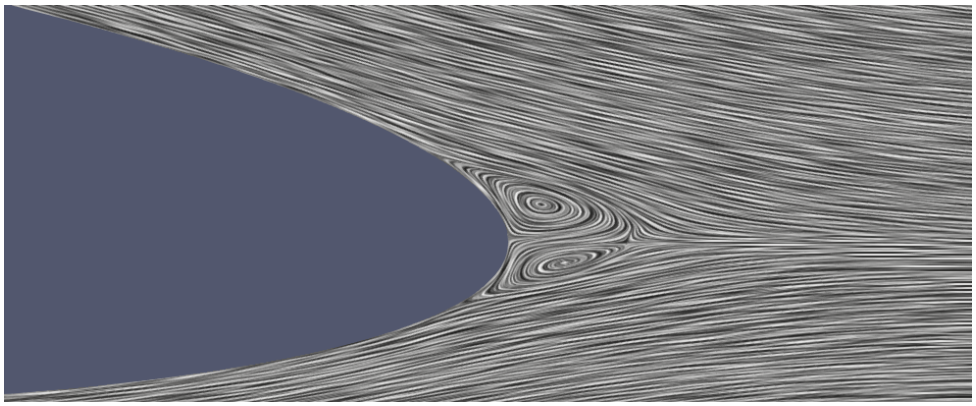

Figure 8: Close-up of near trailing edge flow for bisymmetric airfoil showing flow separation for an angle of attack of 5 degrees.

4. Results and discussions

Figure 9 shows lift coefficients and aerodynamic effectiveness for all airfoils over a range of angles of attack. The resulting aerodynamic performance parameters are summarized in Table 2. As expected, none of the bidirectional airfoils outperform the baseline airfoil, NACA65-415, in terms of aerodynamic efficiency. The B-spline airfoil is the closest, with a absolute difference in lift coefficient of approximately 0.2 over the whole range, and a relative difference in maximum lift of 13 %. For the aerodynamic efficiency, the curve for the B-spline airfoil has a similar shape but a slightly shifted profile compared to the baseline airfoil. The peak performance is only 8.4 % lower than the baseline airfoil. In terms of off-design performance, the baseline airfoil has the design point furthest from the stall point with $\Delta\alpha = 10$. The slope of the aerodynamic efficiency is higher for the baseline airfoil with $S_\epsilon = 3.50$ compared to $S_\epsilon = 1.01$ for the B-spline airfoil. A low slope is beneficial as this gives less on the turbine in off-design conditions. However, since the B-spline airfoil has the design point very close to the stall point, the slope becomes artificially low. This illustrates that when considering off-design performance, it is important to take both $\Delta\alpha$ and S_ϵ into account.

The lowest performing airfoil is the symmetric version of the baseline airfoil, SYM65-015. It has an absolute difference in lift of 0.2-0.4 over the full range compared to the baseline airfoil, and the difference in maximum aerodynamic effectiveness is 48 %. Its only remedial feature is that it reaches stall later than the other airfoils, hence the off-design performance is good with $\Delta\alpha = 8$ and $S_\epsilon = 1.83$.

The asymmetric airfoil, ASYM65-415, has a similar aerodynamic efficiency as the B-spline airfoil at lower angles of attack, with an absolute difference in lift of only 0.07. However, the asymmetric airfoil reaches stall at a lower angle of attack of approximately 11° compared to 15° for the B-spline airfoil. Hence its operating range in a stall-regulated turbine is lower than the B-spline airfoil.

The reduced stall performance is further illustrated in Figure 10, which shows the pressure coefficient and the flow pattern around the asymmetric airfoil and the B-spline airfoil for an angle of attack of 12 degrees. The B-spline airfoil clearly has lower pressure on the suction side at the leading edge giving higher lift. Additionally, there is no separation along the airfoil expect a small section at the trailing edge, which is unavoidable due to the nature of a reversible airfoil. For the asymmetric airfoil the flow separates earlier towards the trailing edge, resulting in reduced aerodynamic performance.

Table 2: Aerodynamic parameters for the airfoils.

Airfoil	$\epsilon_{\max}$ (-)	$C_{L,\text{design}}$ (-)	$C_{L,\max}$ (-)	$\Delta\alpha$ (°)	S_ϵ ($^{\circ -1}$)
NACA65-415	59.2	0.98	1.50	10	3.50
SYM65-015	38.9	0.76	0.90	8	1.83
ASYM54-415	46.3	0.67	0.86	4	3.25
B-spline	54.5	1.11	1.30	4	1.01

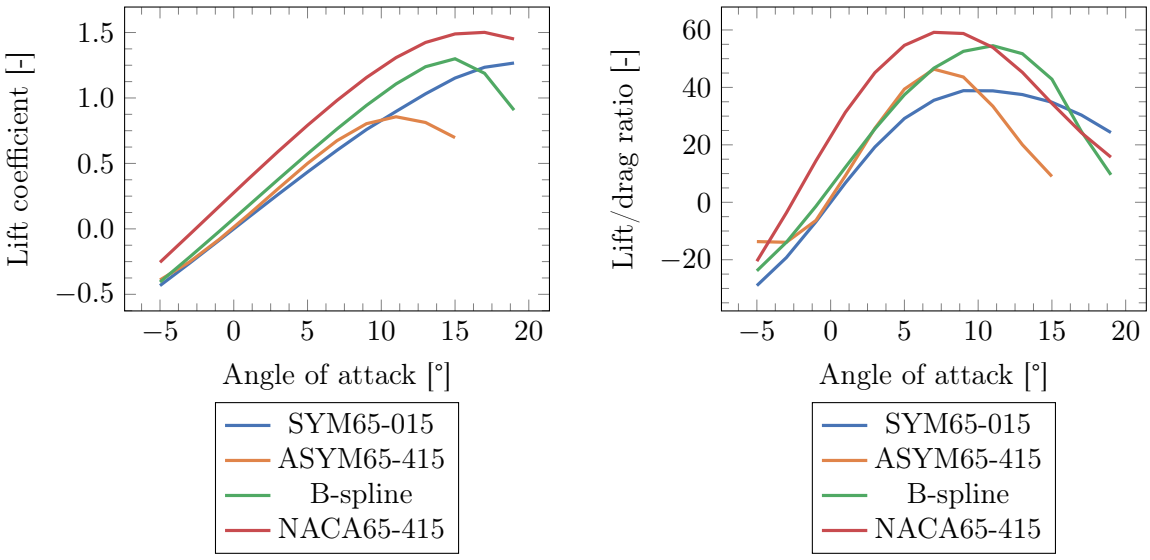

(a) Lift coefficient. **(b)** Lift/Drag ratio.

Figure 9: Simulated coefficients for all airfoils.

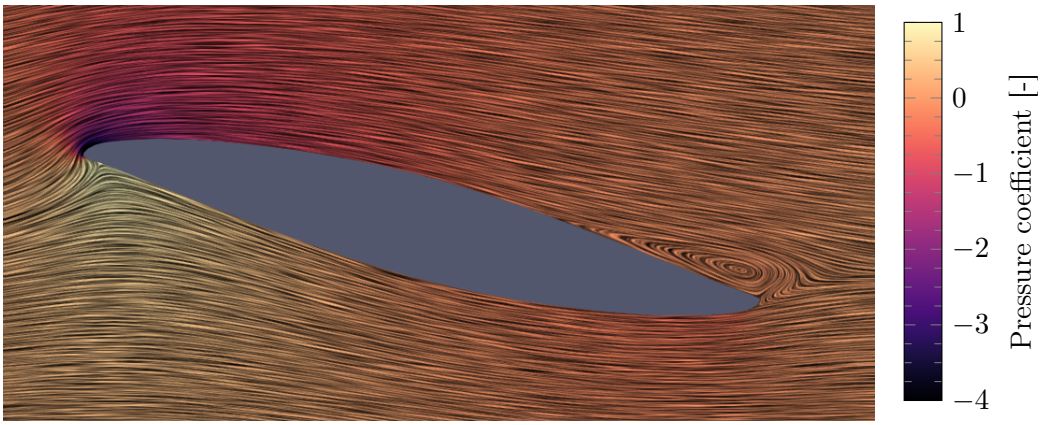

(a) ASYM65-415 airfoil.

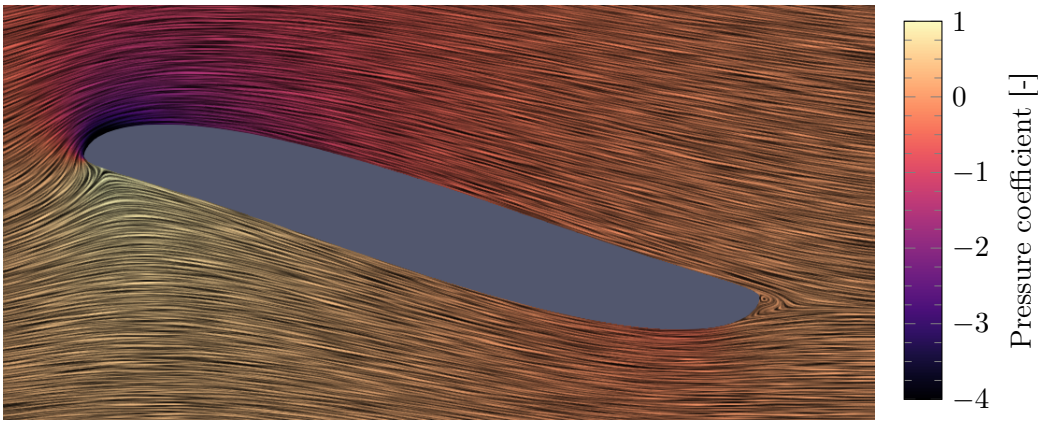

(b) B-spline airfoil.

Figure 10: Pressure coefficient and flow pattern for ASYM65-415 and B-spline airfoils at an angle of attack of 12 degrees.

5. Conclusion

This work investigated the aerodynamic performance of some selected reversible airfoils using computational fluid dynamics. The selected airfoils were based on existing NACA 6 profiles and a profile using B-spline parameterization. The performance parameters of the airfoils included maximum aerodynamic efficiency as well as robustness for off-design conditions. The results show reduced performance for the reversible airfoils compared to a unidirectional airfoil. Of the investigated airfoils, the B-spline airfoil has the highest performance, with a maximum aerodynamic efficiency which is 87 % of the unidirectional design.

Future work will consider the use of an optimization method to further improve the performance of the B-spline airfoil.

Acknowledgments

We acknowledge Maryam Ghorbani for fruitful discussions regarding this work.

References

[1] Angelini G, Bonanni T, Corsini A, Delibra G, Tieghi L and Volponi D 2018 *Designs* **2** 19
[2] Niemiec R J, Jacobellis G and Gandhi F 2015 Leading-and trailing-edge reversal of a cambered airfoil for stopped rotors *56th AIAA/ASCE/AHS/ASC Struct, Struct Dyn Mat Conf*
[3] Heo Y G, Choi N J, Choi K H, Ji H S and Kim K C 2016 *Energ Buildings* **129** 162–173
[4] Li L, Chen Y and Wang Z 2013 Numerical calculations of bidirectional characteristics on tidal current runner *ASME IMECE* vol 56291
[5] Nedyalkov I and Wosnik M 2014 Performance of bi-directional blades for tidal current turbines *ASME FEDSM* vol 1C
[6] Guo B, Wang D, Zhou X, Shi W and Jing F 2020 *Water* **12** 22
[7] Li X, Yang K, Bai J and Xu J 2016 *Energy* **116** 202–213
[8] Salunke N P, A J A R and Channiwala S 2014 *Amer J Mech Eng* **2** 99–102
[9] Weller H G, Tabor G, Jasak H and Fureby C 1998 *Comput Phys* **12** 620–631
[10] Jasak H, Jemcov A, Tukovic Z *et al.* 2007 OpenFOAM: A C++ library for complex physics simulations *CMND* vol 1000 (IUC Dubrovnik Croatia)
[11] Spalart P and Allmaras S 1992 A one-equation turbulence model for aerodynamic flows *30th Aerospace Sciences Meeting* p 439
[12] Sweby P K 1984 *SIAM J Numer Ana* **21** 995–1011
[13] Presser D 2013 Construct2D - COmputational fluid dyNamics STRUctured grid CreaTor for 2D airfoils `https://sourceforge.net/p/construct2d/code/ci/v2.0.3/tree/` accessed: 2021-08-06
[14] Hoerner S F and Borst H V 1975 *NASA STI/Recon Tech Rep A* **76** 32167
[15] Rumsey C 2021 2DN00: 2D NACA 0012 airfoil validation case `https://turbmodels.larc.nasa.gov/naca0012_val.html` accessed: 2021-08-06
[16] Ladson C L 1988 *Effects of independent variation of Mach and Reynolds numbers on the low-speed aerodynamic characteristics of the NACA 0012 airfoil section* vol 4074 (NASA Langley Research Center)